Effects of liquid properties on atomization and spray characteristics studied by planar two-photon fluorescence

Cite as: Phys. Fluids **34**, 083305 (2022); https://doi.org/10.1063/5.0098922
Submitted: 13 May 2022 • Accepted: 06 July 2022 • Published Online: 04 August 2022

Published open access through an agreement with Universität der Bundeswehr München Fakultät für Luft- und Raumfahrttechnik

Hannah Ulrich, Bastian Lehnert, Diego Guénot, et al.

Physics of Fluids ARTICLE scitation.org/journal/phf

Effects of liquid properties on atomization and spray characteristics studied by planar two-photon fluorescence

Cite as: Phys. Fluids **34**, 083305 (2022); doi: 10.1063/5.0098922
Submitted: 13 May 2022 · Accepted: 6 July 2022 ·
Published Online: 4 August 2022

View Online Export Citation CrossMark

Hannah Ulrich,[1,2,a)] Bastian Lehnert,[2,3] Diego Guénot,[4] Kristoffer Svendsen,[4] Olle Lundh,[4] Michael Wensing,[2,3] Edouard Berrocal,[2,5] and Lars Zigan[1,2]

AFFILIATIONS

[1]Institut für Thermodynamik, Professur für Energiewandlug, Fakultät für Luft- und Raumfahrttechnik, Universität der Bundeswehr München (UniBw M), Neubiberg, Germany
[2]Erlangen Graduate School in Advanced Optical Technologies (SAOT), Friedrich-Alexander-Universität Erlangen-Nürnberg (FAU), Erlangen, Germany
[3]Professur für Fluidsystemtechnik (FST), Friedrich-Alexander-Universität Erlangen-Nürnberg (FAU), Erlangen, Germany
[4]Division of Atomic Physics, Lund University, Lund, Sweden
[5]Division of Combustion Physics, Lund University, Lund, Sweden

Note: This paper is part of the special topic, Development and Validation of Models for Turbulent Reacting Flows.
[a)]**Author to whom correspondence should be addressed:** hannah.ulrich@unibw.de

ABSTRACT

In this work, planar two-photon laser-induced fluorescence (2p-LIF) is applied for the first time to analyze the fluid dependent spray structure and atomization behavior of water and ethanol in a quantitative way. A commercial six-hole DISI (Direct-Injection Spark-Ignition) injector was studied at different injection pressures, operated with liquids containing the LIF dye fluorescein. Specifically for DISI-injectors, the fluid-dependent atomization is very complex and not fully understood due to the cavitating, turbulent nozzle flow that dominates the spray formation. Optical access and analysis of the near-nozzle spray are often challenging due to multiple light scattering in dense regions which is reduced by 2p-LIF measurements using a femtosecond laser. This allows high-contrast spray imaging close to the nozzle, resulting in an improved identification of single liquid structures of the spray. Thus, a higher accuracy of sizing is possible. Compared to water, the ethanol spray shape shows increased cone angles in the nozzle near-field of about 6%, which cannot be explained by classical atomization theory based on aerodynamic breakup. The larger cone angle of ethanol was attributed to its larger viscosity, which could decelerate the flow at the wall of the injection hole, affecting the velocity profile of the emerging jet. The atomization shows a main jet breakup distance of 7–10 mm in which the structure sizes decreased drastically, specifically for water. For the size of the liquid structures in the near-nozzle region, which show dimensions of about 80–130 μm, ethanol exhibited about 2% smaller Feret's diameters than water for the tested time steps at 20 MPa. This effect is even more distinct for other injection pressures and positions at a further distance to the injector. For all investigated conditions and measurement positions downstream of the nozzle, ethanol showed on average about 24% smaller structures compared to the water spray. Although this trend is in accordance with the classical atomization theory based on the aerodynamic breakup mechanism, other effects, such as cavitation and nozzle-flow induced breakup, contribute to this behavior.

INTRODUCTION

Atomization of liquids and spray formation is particularly important for fuel injection in IC engines, rocket engines, or gas turbines since the efficiency of the combustion process is determined by the rapid fuel evaporation and mixture with oxidizer.[1,2] Controlling and optimizing atomization, fuel dispersion,[3] and evaporation through a well-designed injection system allows reducing fuel consumption as well as pollutant emissions such as nitric oxides (NO_x) or soot.[4,5] A well-controlled atomization is also important for other injection processes,[1] such as powder generation from spray drying, printing,[6] surface coating,[7] flame spray pyrolysis, or spray cooling.

For optimization of atomizers and spray processes, an enhanced understanding of the complex fluid dynamics inside and outside of the nozzle is required. Furthermore, liquid properties determine the internal nozzle flow, the atomization, and spray structure. For example, in combustion applications such as IC engines, aircraft engines, or gas turbines, the application of modern biofuel and synthetic fractions may vary the nozzle flow and atomization, which again determine evaporation, mixing, and combustion behavior.[5,8]

The injection system should be also capable to atomize different liquids with comparable quality in order to enable, e.g., ignitability in the case of combustion applications. For example, Qavi and Jiang reported a poor ignition performance of highly viscous fuels for some injectors.[9] This can be due to the limited viscosity tolerance of the applied fuel injection systems. For example, the pressure swirl injector is able to produce narrow size distributions, but just for fuels with low viscosity and surface tension.[10] The atomization of this injector type is solely based on aerodynamic breakup, which is also true for air blast injectors. In these "classical" injectors, droplets are generated following the Kelvin–Helmholtz (KH) or Rayleigh–Taylor (RT) induced instabilities on the interface between liquid and gas. These wave-like disturbance on the jet (and/or droplet) will break up into ligaments and lead subsequently to droplet detachment[11,12] as depicted in Fig. 1. In principle, the surface wave amplitude rises with increasing relative velocity between the liquid and the ambient gas flow. Contrary, these oscillations are damped by the viscosity of the fluid so that this fluid property is a limiting factor for fine atomization. This aerodynamic-induced droplet formation process is relatively well understood, and models (e.g., the "wave model"[13]) are widely applied in computational fluid dynamics (CFD) packages. Additionally, most of the published direct numerical simulation (DNS)-like simulations of the jet disintegration are based on this breakup mechanism.[14]

However, the influence of the inner nozzle flow on jet atomization is often not considered.[16] Specifically, turbulent fluctuations in the nozzle flow may lead to initial disturbances on the liquid jet that promote its disintegration. Those turbulence-induced surface waves at the nozzle grow subsequently due to aerodynamic instabilities of the liquid jet.[17] Figure 1 illustrates the spray breakup due to aerodynamic influences and also cavitation inside the nozzle. Transient two-phase flows occur specifically in diesel or gasoline injectors due to cavitation.

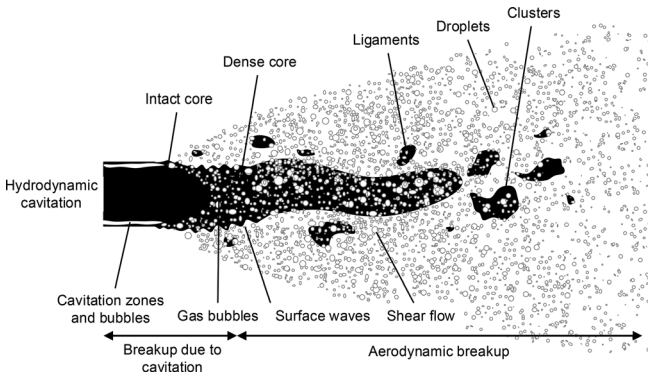

FIG. 1. Spray breakup model with aerodynamic and cavitation induced breakup after.[15]

In the subsequent paragraphs, a short review of cavitation in diesel and gasoline nozzles is presented, as these two-phase flows determine the spray formation at the injector outlet. The breakup in the near-nozzle field is the focus of the present paper. The cavitating flow inside the injector is not accessible with the present optical setup of this paper. However, some fundamentals of cavitation are necessary in order to understand the cavitation-induced breakup and the origin of cyclic variations in the spray under investigation.

Specifically, in high-speed diesel nozzle flows, two-phase regions are generated due to cavitation.[18] "Geometric cavitation" occurs specifically near the sharp corner of a hole inlet where the pressure drops locally below the vapor pressure of the fuel.[19] The collapse of vapor bubbles at the nozzle outlet again leads to strong turbulence supporting ligament formation in the liquid jet. Specifically for geometric cavitation conditions, a large part or the whole nozzle hole surface may be covered with vapor so that the wall is not in contact with liquid fuel. This results in a very slim jet at the nozzle outlet, which is known as "hydraulic flip." This slim jet does not show large surface waves, which also indicates that the simple presence of cavitation does not guarantee jet disintegration.[20]

Furthermore, specifically at high pressure and in high velocity flows occurring under diesel injection conditions, geometric cavitation leads to erosion in the nozzle, and this must be avoided,[21] for example, by conical nozzle holes. Consequently, the atomization process in diesel jets is realized less by cavitation but mainly due to aerodynamic and turbulence-induced breakup. For direct injection spark ignition (DISI, often just called "gasoline direct injection") conditions, cavitation is a very relevant atomization process. The two-phase flow in the nozzle already contains a high amount of gas (vapor and entrained ambient gas, contrary to diesel primary jets) so that the actual jet disintegration is initiated inside the nozzle and the typical step-hole of current injector geometries. This is confirmed by CFD-simulations and x-ray measurements.[22,23] For example, Guenot *et al.* determined a maximum liquid volume fraction of water at the exit of the DISI nozzle of 55% and a rapid atomization of the liquid jet by using laser-plasma-driven x-ray transmission radiography measurements.[22] Here, a multi-hole nozzle was analyzed with a step-hole geometry. CFD simulations resulted in vapor fractions at the nozzle outlet of a DISI three-hole injector in the range of about 5%–11%[23] depending on the needle lift and the fuel (n-hexane and n-decane were tested in this case). However, in this simulation, only cavitation was considered without any gas entrainment into the nozzle, which is promoted by step-hole nozzles. Both the simulation and the experiments (microscopic planar Mie-scattering was conducted at the nozzle outlet) confirmed the existence of string cavitation (vortex type cavitation) and large cavities in the liquid fuel jet. String cavitation is another type of vapor formation in the nozzle.[24] It occurs in low pressure regions in the liquid bulk, which can be a consequence of large-scale vortices produced in the nozzle sac or nozzle hole. These cavitation structures propagate into the injector hole determining the flow of the liquid jet at the outlet of the nozzle. The formation of cavitation strings is very irregular. These structures may affect the cone and bend angle of the jet and strongly support spray instabilities such as cyclic spray variations,[23,25] i.e., the spray targeting and width varies from injection to injection. This means the atomization and liquid fuel distribution also varies from injection to injection, which is another disadvantage of cavitation. In addition to the variation of the spray angle, cavitation may lead to an

increase in the velocity of liquid jet, which is due to a reduced effective hole diameter. This may also vary from injection to injection and contributes to cyclic spray shape variations.

This complex atomization and spray behavior can hardly be predicted by semi-empirical breakup models that are included in CFD software packages. Most of these atomization models mainly take aerodynamic breakup effects into account and fewer also consider turbulence- or cavitation-induced breakup. However, the instationary nozzle flow may superimpose and even control the aerodynamic breakup, so that the atomization process is not fully understood. In principle, there are many studies focusing on aerodynamic breakup for various liquids; however, in these cases, usually the nozzle flow is relatively simple and cavitation effects play a minor role. For example, recently Qavi and Jiang studied the effects of fuel properties on the near nozzle spray characteristics of a twin-fluid injector.[9] The base jet-A fuel (kerosene) with a low viscosity was compared to two higher viscous fuel blends. A similar atomization completion length of about four times the nozzle diameter (4D) downstream the nozzle was detected for all fuels. The final droplet size is 6% to 10% larger for the higher viscous fuels than for the base fuel. From these observations, the authors concluded that surface tension and liquid density do not have a significant effect on the breakup.

Contrary results were presented by Tareq *et al.* who studied air blast atomization of water compared to kerosene.[26] The surface tension of water is much larger than for kerosene, while the dynamic viscosity is doubled for kerosene. This resulted in larger droplet sizes for water and larger cone angles for kerosene. It was concluded that the surface tension effects are more significant than the viscous effects for this liquid sheet breakup mode being controlled by Kelvin–Helmholtz instabilities.

Reitz and Bracco studied the effects of dynamic viscosity on the jet cone angle for different nozzle geometries and injection conditions.[20] They found a decrease in the jet angle with increasing liquid dynamic viscosity. This trend can mainly be explained by aerodynamic breakup theory and fits roughly to respective phenomenological models. However, it was also mentioned that different nozzle geometries with varied flow profiles and onset of cavitation could lead to deviations from this behavior.

As mentioned above, the nozzle flow cannot be neglected in the case of cavitation and distinct turbulence, which complicates the modeling of atomization processes. In general, there are a few works and correlations of fuel dependent cavitation and turbulent nozzle flow on the spray shape and atomization.[23,27,28] Both cavitation and turbulence increase with lower viscosity[28] determining the liquid flow, specifically the axial and radial velocity field at the outlet. For example, a lower liquid viscosity may accelerate the liquid flow exiting the nozzle also at the nozzle wall. This may lead to larger injection velocities and to a reduced spray cone angle for the lower viscosity fuel as shown for n-hexane, in comparison to higher viscous n-decane for a DISI injector in Ref. 23. Furthermore, this is opposed to the study of Reitz and Bracco mentioned above.[20] For the lower viscosity fuel, fewer large structures (ligaments, clusters) were observed in the near-nozzle region.[23] It was concluded that these fuel-dependent effects cannot be described by the aerodynamic breakup alone. Contrary, the spray shape is mainly determined by the highly unsteady, cavitating nozzle flow and specifically by the developed flow profile at the nozzle outlet, which again depends on the viscosity of the liquid. This liquid property also determines cyclic variations of the spray shape and targeting. However, the effects of the surface tension on the spray shape and ligament formation could not be clearly identified, and only injection pressures of 5 and 10 MPa were studied.[23]

Consequently, there are still many open questions on dependencies of liquid properties on the spray formation for various injectors and conditions. Thus, the analyzation of such sprays is useful for a further understanding of atomization in manifold energy and process engineering applications. In spray imaging, there are a great variety of approaches to examine the characteristics of the liquid jets. The range of conventional methods extends from macroscopic and microscopic imaging over planar and tomographic measurements to qualitative and quantitative analyzations. Each region of the spray has a different characteristic (e.g., liquid volume fraction, droplet number, etc.), and thus variable visualization techniques have emerged in the last decades.[29] As for the nozzle near-field, the sprays are usually very dense, and hence the illumination and detection of the spray structure suffer from multiple light scattering. The majority of the detected photons have been scattered multiple times by ambient off-axis liquid structures. This effect leads to a masking of the investigated liquid structures in the core spray.[29–31]

In recent years, various measurement techniques such as x-ray radiography, ballistic imaging (BI), or structured laser illumination planar imaging (SLIPI) have been established for the attempt to suppress multiple scattering.[30,32,33] One approach to circumvent the detection of multiply scattered photons is to suppress the light, which is scattered by structures from outside of the focus plane. For example, in BI, the photons refracted by large fluid structures are preserved, while multiply scattered photons are filtered by a temporal gate to avoid misleading effects.[33,34] Another way to correct corruption of the data is filtering the erroneously detected photons in the post processing. This method is applied in SLIPI where a spatially modulated laser sheet is used to visualize the spray.[35,36]

In a previous work, Guénot *et al.*[31] introduced the combination of x-ray and 2p-LIF measurements to get insight into the detailed spray structure. Both techniques avoid the generation of multiple scattering, and thus the intensity of the ambiguous off-axis signals is insignificant. A comparison between the usual one- and the used two-photon fluorescence is depicted in Fig. 2.

The approach of 2p-LIF is based on the probability of a simultaneous absorption event of two photons. This probability is high in the focus plane, where the liquid structures absorb the fs-laser light and emit fluorescing photons. In the turbid spray region outside of the laser light sheet, the scattering effects occur with a wide spatial and temporal distribution. Consequently, the energy of an absorbed photon in the fluorescence dye is insufficient to elevate electrons from their electronic ground state to an excited state. This means that the dye will not show fluorescence in the case of one-photon excitation. Only two-photon excited dye molecules will show fluorescence, which leads to high-contrast spray imaging close to the nozzle, resulting in an improved identification of single liquid structures compared to conventional LIF techniques. The planar detection of the signal from a thin laser sheet allows a precise sizing of liquid structures, which is not possible in dense sprays with line-of-sight techniques such as shadowgraphy,[11,37] BI or x-ray radiography.[22] 2p-LIF has been widely applied in, e.g., biological microscopy[38] or in flame species measurements.[39–41] Berrocal *et al.*[30] introduced this technique to visualize atomizing water

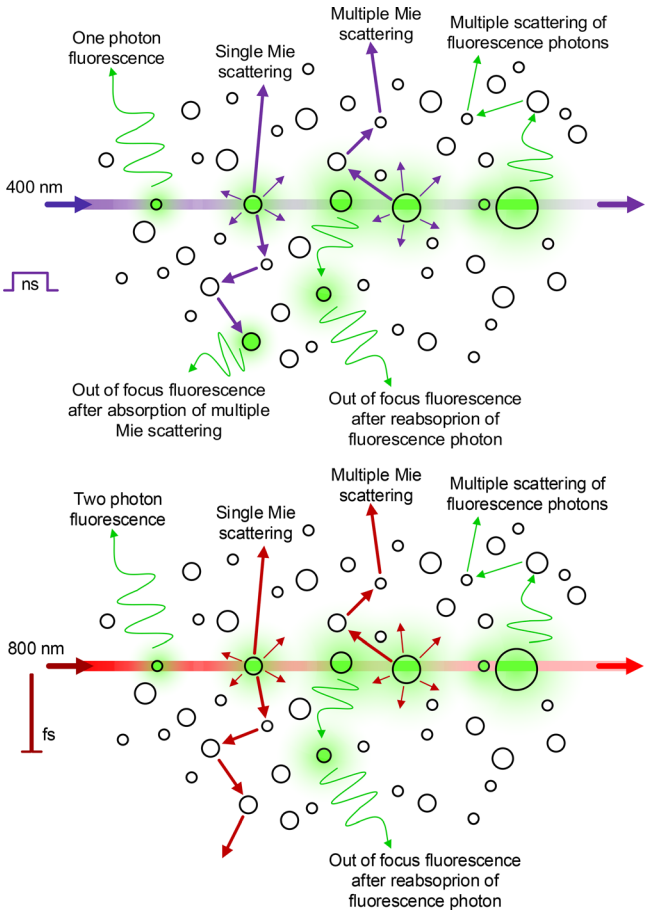

FIG. 2. Comparison of single- (top) and two-photon (bottom) laser induced fluorescence following Ref. 30. Note that different excitation laser wavelengths are applied.

sprays and presented a comparison to the common single-photon LIF approach.

In this work, we continued the investigations by operating the injector with different liquids at different injection pressures with a detection at various points in time during the injection [after the visible start of injection (vSOI)]. As mentioned above, the fluid properties like surface tension and viscosity determine the size, shape, and local distribution of the resulting liquid spray structures, as well as the spray width and cone angle. Furthermore, they control cyclic variations of the spray shape and targeting, which again determines the atomization quality, droplet dispersion as well as the subsequent mixing process.

Two fluids are selected with distinct differences in surface tension and viscosity. Different injection pressures of a DISI injector are studied to realize larger relative velocities that determine atomization especially in terms of aerodynamic breakup. Water and ethanol are selected as they are both common solvents in various spraying processes such as painting, cooling, particle synthesizing, and fuel combustion. Ethanol is a relevant synthetic fuel or biofuel for automotive or aerospace application. Water is also applied in combustion or industrial applications including exhaust gas after treatment (in mixtures with ammonia for selective catalytic reduction of nitrous oxides, NO_x) or water/oil or water/fuel emulsions.[42] Water/fuel emulsions are promising for IC engine applications specifically at higher loads for improved fuel efficiency. Usually, fuel and water are injected separately with different injectors, but the injection of a mixture with different water content (depending on the engine load, with larger water concentration at higher load) using the same injection system would be advantageous.[43] In the case of emulsions, ethanol is also a promising solvent to stabilize the fuel/water mixture.[44] The microscopic spray shape was analyzed in the near-nozzle region using two photon LIF. These experiments can provide conclusions on the near-nozzle flow and primary spray formation for a detailed comparison of the fluid-dependent breakup process and the resulting liquid structures in dense sprays. Dimensions of liquid structures such as ligaments and clusters are determined based on the Feret's diameter in different positions downstream the nozzle and at various points in time after start of injection. The microscopic spray shape is analyzed in this paper via the cone angle, which is also discussed in terms of cyclic variability.

MATERIAL AND METHODS

The measurements were performed using a titanium-sapphire chirped pulse amplification system at Lund High-Power Facility, being further described in Ref. 45. The light intensity needs to be sufficient to overcome the energy gap of the fluorescent molecules with two photons. Therefore, the femtosecond laser generates pulses with a pulse energy of 10 mJ and a duration of 38 fs. With a center wavelength of 800 nm, two photons match the necessary energy for a two-photon fluorescence of the LIF dye fluorescein. A fraction of 0.1% fluorescein is added to both investigated liquids, water and ethanol. According to Guénot *et al.*, the equivalent fuel properties were determined to be unaffected by adding only this small amount of dye.[31] Additional measurements were conducted and showed no difference in dynamic viscosity and surface tension. Regarding the density, the mixture of ethanol with the dye shows a slight but negligible deviation of the density of pure ethanol. For the measurements, a commercial six-hole DISI injector with one optically clearly separable (as some jets overlap in some perspectives) definable spray cone is studied. It should be noted that a single-hole nozzle would provide better optical access. However, a single-hole injector or the blocking of individual nozzles of a multi-hole injector would lead to a changed and nonrealistic internal nozzle flow (i.e., varied turbulence and cavitation in the sac hole and injection holes) as well as spray behavior. Furthermore, a blocking of single holes could potentially result in a destruction of the injector.

The considered nozzle has a diameter of 100 μm. The injector is operated at the three different injection pressures of 10, 20, and 30 MPa. By increasing the pressure, a larger liquid mass is injected. Four different points in time after the visible SOI are recorded.

The imaging system of the setup is depicted in Fig. 3. A cylindrical lens with a focal length of 150 mm was utilized to generate a light sheet of ~2 cm × 100 μm at the nozzle exit. The detection system consists of a telecentric lens combined with a high resolution 5.5 megapixel sCMOS camera (Andor Zyla 5.5) resulting in a resolution of 6.5 μm/pixel.

For additional comparison, further images are taken with backlight illumination. For this purpose, the laser beam was directed straight to a fluorescing background behind the spray. Hence, the detection system collects a shadowgraphy image of the spray in that case, i.e., an integral spray image is taken. These

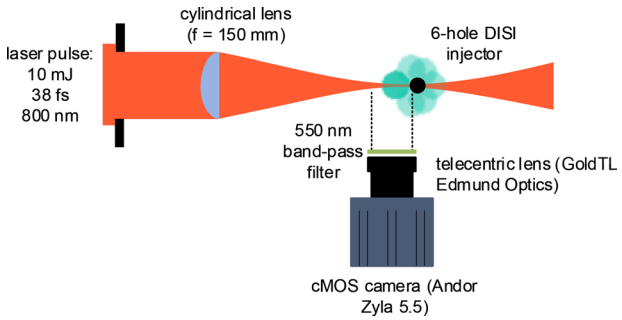

FIG. 3. Optical setup for the 2p-LIF measurements.

images are only used to reassess the information obtained by the 2p-LIF measurements.

The LIF images are post-processed with a routine in the software package ImageJ, which consists of a binarization of the maximal recorded 50 single-shot raw images, see Fig. 4. For this purpose, an intensity threshold of 25/255 is set for the converted eight-bit pictures, according to the method of Zantow *et al.*[46] This value is determined to separate between in-focus liquid structures (for signal intensities $\geq$25) and "background/noise signal" (for signal intensities $<$ 25). The latter consists of camera noise and possibly fluorescence signal of very small droplets in the plane of the laser sheet. For the threshold determination, several methods were tested, and the above stated value of 25/255 was found to be optimum.

For the determination of the near-field cone angle, a linear interpolation of the radial spray boundary is conducted from the nozzle exit up to a 1 mm distance from the nozzle. The angle of the spray is measured within this region for the single-shot images. A 95% confidence interval is calculated using Student's t-distribution.

Additional post-processing provides information about the dimensions of the liquid structures located in the area up to 4 mm distance downstream the nozzle exit. An analysis of all structures with an overall size $>$15 arbitrarily connected pixels rejects droplets and small ligaments to reduce an overestimation of the size due to the resolution. All larger structures are evaluated by measuring Feret's diameter, which is the maximum distance between any two points of the liquid body.

The Feret's diameter is also analyzed downstream in 0.5 mm steps from the nozzle exit. As the liquid structures in the nozzle far-field are smaller, compared to the ones in the 4 mm surrounding of the nozzle, the rejection threshold is lowered to 10 pixels. Thus, the considered structures exceed the size of 3 $\times$ 3 pixels, which is a common accuracy limit for sizing of liquid structures.[47,48]

For the angles and the Feret's diameters, values of all recorded single images are determined and averaged afterwards.

RESULTS AND DISCUSSION

Figure 5 shows enlargements of the liquid structures of a water and an ethanol spray. With the suppression of multiple light scattering, the main advantage of the two-photon approach, it was possible to image the structure of an optically dense liquid jet of a single spray plume near the nozzle. Generally, the recorded images provide deep insights into the atomization behavior including the emerged formations of ligaments, clusters, and droplets. These structures may be hidden or blurred and thus optically distorted when other planar 1p-LIF techniques or Mie-scattering are utilized. However, in these 2p-LIF-images, some fluorescence signal is visible in the right part of the plume, which also appears blurred. In these areas, the spray plume merges with the other jets (which is known as jet-to-jet interaction). The fluorescence signal originates from small droplets emanating from the out of focus spray plumes. These small structures refract the light randomly and not in unison. The spatial and temporal dispersion of secondary scattered fluorescence photons could also lead to a LIF signal in these regions. An attenuation of the fluorescence signal can be related to reabsorption effects of the dense spray partially covering the jet under study.

For clarification of the overlap of the plumes and jet-to-jet interaction, an exemplary shadowgraphy image is shown in Fig. 6 in comparison to an inverted raw 2p-LIF intensity image. By including the shadowgraphy images, the position of the adjacent off-axis spray cones is estimated. In the region of the single spray plume under investigation, the fluorescence image shows a clear signal. As for the interference with the remaining spray jets, the fluorescence intensity signal gets blurry and prevents a clear separation of the single plumes.

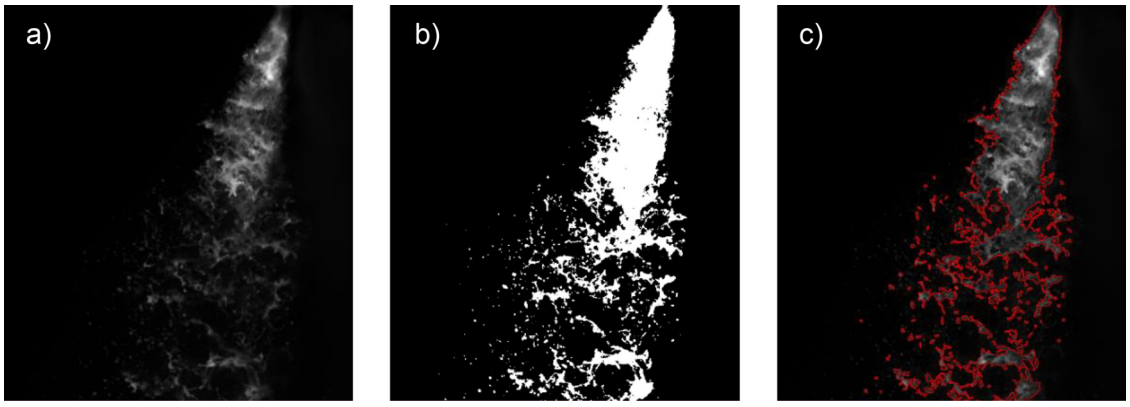

FIG. 4. Post processing of the images. (a) shows the original image, (b) the binarized structures, and (c) the contours superimposed with the original picture.

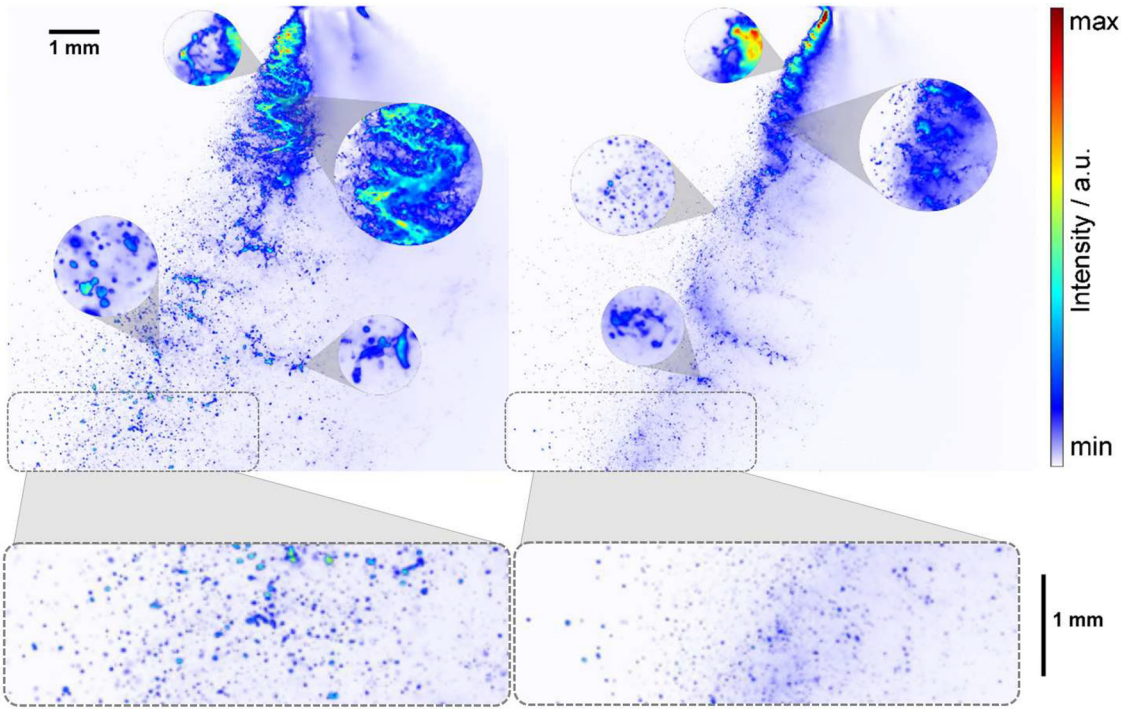

FIG. 5. Liquid fuel structure of a single plume of a water (left) and an ethanol spray (right) including magnifications of ligaments, wavy jet breakup zones, clusters, and droplets in the nozzle near and far-field (marked by separate boxes in the bottom row).

Consequently, in the subsequent analysis, the spray cone angle is related to the left boundary of the spray and the injector body axis (vertical line from nozzle exit). The width of the spray plume cannot be determined reliably.

Figure 7 depicts the sprays at 20 MPa, and this between 20 and 320 μs after visible injection start. Until the first pictures are taken at 20 μs, no distinct atomization takes place, and for both liquids, no ligaments are formed yet. In the latter time steps, the difference in the liquid breakup gets clearly visible, showing larger structures and oscillating/wavy jets in the water spray. After 220 μs, the spray exceeds the light sheet and the spray front cannot be tracked further. Since the spray images are taken for different injections, the development of the spray shape (esp. the spray width) is also superimposed with effects of cyclic variations.

Figure 8 shows the second picture series with single shots of ethanol and water sprays at three different injection pressures, all at 220 μs. With increasing pressure, the spray core breaks up faster, leading to smaller structures and a shorter spray penetration.

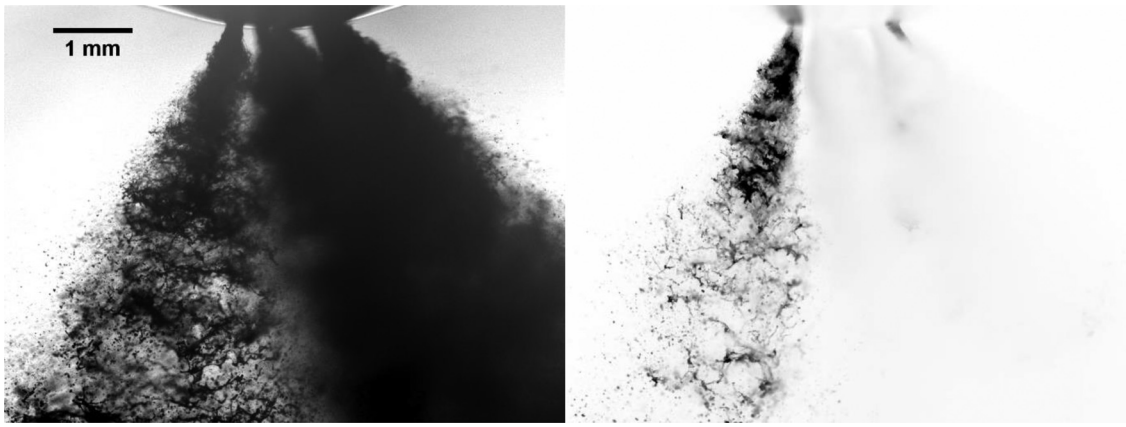

FIG. 6. Shadowgraphy image (left) and an inverted 2p-LIF image (right) of the water spray at 20 MPa and 220 μs after vSOI. Only spray structures at the left side of the single spray plume can be analyzed using 2p-LIF due to overlap of single plumes that may disturb optical access.

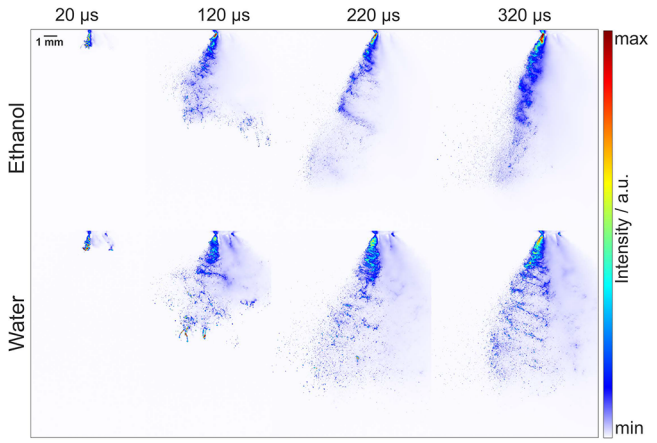

FIG. 7. Single shot LIF images for ethanol and water sprays at different detection points in time after vSOI at an injection pressure of 20 MPa.

Due to an increasing liquid pressure, a larger liquid mass is injected and the opening behavior of the needle changes. This leads to an increase in the ligament size and very large structures in the spray front specifically at 30 MPa. Mainly, the water spray shows an increased number of large structures in the form of blobs and sheets, which is also distinct at 30 MPa. Obviously, the breakup into smaller droplets is more efficient for ethanol. These resulting structure dimensions and droplet sizes would also affect the subsequent processes evaporation and mixture formation. In the next paragraph, the effects of the fluid properties on the spray shape and structure are analyzed in more detail.

Two main properties determining the nozzle flow and atomization are the viscosity and the surface tension. Density and vapor pressure of the liquids are provided as well. A larger vapor pressure will promote cavitation (geometric and string cavitation). The values are shown in Table I.

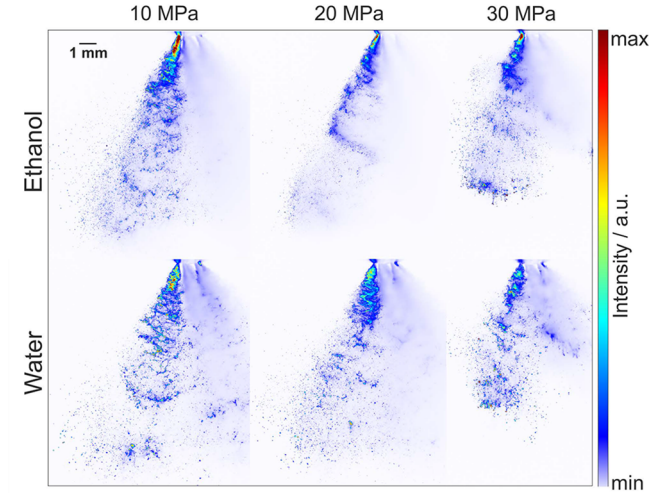

FIG. 8. Single shot LIF images of ethanol (top) and water (bottom) for an injection pressure variation at a point in time of 220 μs after vSOI.

TABLE I. Fluid properties of ethanol and water at 293 K and 0.1 MPa.[49,50]

	Density (kg/m^3)	Dynamic viscosity (mPa s)	Surface tension (mN/m)	Vapor pressure (kPa)
Ethanol	789.42	1.194	22.39	5.88
Water	998.21	1.002	72.88	2.34

Two pressure dependent dimensionless numbers—the Reynolds (Re) and Weber numbers for liquid flows (We_L)—were determined and are shown in Table II. The Reynolds number is defined by

$$Re = \frac{\rho \cdot D \cdot u}{\eta}, \tag{1}$$

whereas the Weber number can be mathematically formulated as

$$We_L = \frac{\rho \cdot D \cdot u^2}{\sigma}. \tag{2}$$

The included quantities are liquid density ρ, nozzle diameter D, velocity (at nozzle exit) u, dynamic viscosity η, and surface tension σ. The (average) velocity is calculated after Bernoulli's law as conducted in Ref. 51. It reaches values between 120 m/s for 10 MPa and 250 m/s for 30 MPa, depending on density and pressure difference. These values correlate with velocities of Diesel and DISI injectors at similar pressures, analyzed by x-ray phase contrast measurements of Neubauer.[52]

Due to its large surface tension, a significantly smaller Weber number is obtained for water, which will affect the droplet formation. The enlarged sections in Fig. 5 show a difference in drop sizes in the nozzle far-field (i.e., at the spray front). Experiments of Shin *et al.* based on Phase Doppler Particle Analyzer (PDPA) and spray tomography confirm that an increase in surface tension leads to larger droplets.[53] Based on the lower Weber number a comparably slow breakup is expected for water, explaining the larger droplets observed in Fig. 5.[54] With both Re und We_L, the Ohnesorge number (Oh) can be calculated. Eliminating the velocity, it describes the ratio of frictional to surface forces and is defined as follows:

$$Oh = \frac{\sqrt{We_L}}{Re} = \frac{\eta}{\sqrt{D \cdot \rho \cdot \sigma}}. \tag{3}$$

A higher Ohnesorge number indicates a faster liquid jet breakup into smaller droplets. For ethanol, an Oh number of 0.028 is received, while

TABLE II. Calculated values for Reynolds and Weber numbers at different injection pressures.

	10 MPa	20 MPa	30 MPa
Re			
Ethanol	9473	13 397	16 407
Water	12 696	17 955	21 990
We_L			
Ethanol	72 367	144 733	217 100
Water	22 228	44 457	66 685

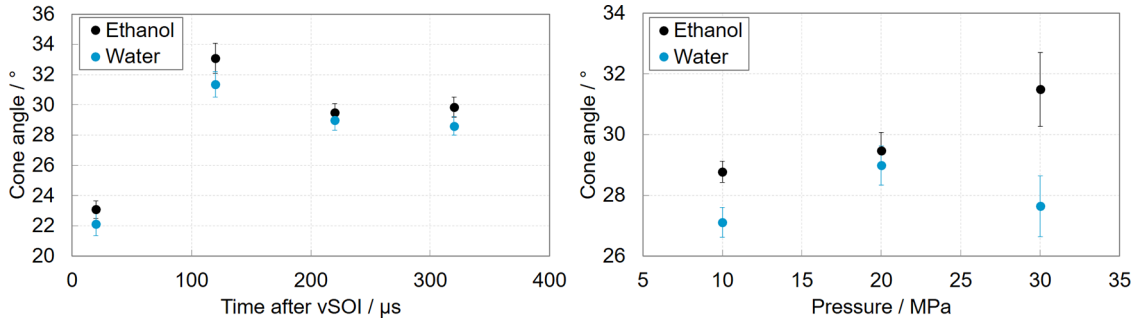

FIG. 9. Time dependent spray cone angle at 20 MPa (left) and injection pressure dependent cone angle at 220 μs (right) with 95% confidence interval.

for water the Ohnesorge number is 0.012. According to the Ohnesorge-diagram, this means that the breakup mode is closer to the "2nd wind-induced regime" for water, while it is clearly in the atomization regime for ethanol. Thus, by trend a faster breakup and smaller droplets are expected for ethanol. This coincides qualitatively with the spray images and a quantitative analysis is presented below in terms of the Feret's diameter of liquid structures.

The Reynolds number is also relevant for the nozzle flow, which determines cavitation and the turbulence-induced breakup. Re is more than 30% larger for water than it is for ethanol. As for the fluid behavior, increased turbulence and cavitation inside the nozzle are expected for larger Reynolds numbers. This may lead to a reduced cone angle according to references.[23,28]

The determined spray cone angles are provided in Fig. 9 at various points in time (left) and for various injection pressures (right). As anticipated, the resulting spray angles for water are smaller for all injection pressures and points in time studied due to the lower liquid viscosity.

Regarding the time-dependent behavior, both liquids show a similar trend. The incipient nozzle near-field cone angle is small, while in the subsequent time step, a strong increase is observed, which can be explained by the increasing flow velocity and developing flow profile during needle opening. It can be assumed that the axial injection velocity is roughly doubled between part lift ($\sim$10 μm) and full needle lift, see, e.g., Ref. 23. When the injector is fully opened (i.e., the needle is completely lifted, which occurs at about 220 μs), the nozzle flow is in a more stationary phase leading to a further decline of the cone angle (by about 8%–12%) and reduced confidence intervals with advanced time (compare, e.g., 120 and 220 μs), see Table III. In Ref. 55, it is argued that the larger cone angle during needle opening is due to a more distinct cavitation. The larger relative vapor fraction in the injection hole due to cavitation during partial needle lift was also confirmed by Zigan *et al.*,[23] who also showed lower cone angles at full needle lift conditions in the stationary phase.

Now, the spray cone angle is studied at 220 μs for the two liquids and injection pressures. This is a relatively early point in time of the spray formation, but the integral macroscopic spray shape (especially spray length and width) is determined in this period. The angle of the ethanol spray at 220 μs is again always larger (on average 7.3%) than the one of water and it shows a steady increase with rising injection pressure. This is probably due to two reasons: First, the higher viscosity (and lower Reynolds number) leads to a more distinct flow deceleration at the nozzle wall and larger velocity gradients at the radial boundary of the emerging fuel jet. For ethanol, the flow is in the transition region and behaves more "laminar-like," which could result in larger spray cone angles.[23,28] Second, and additionally, the aerodynamic breakup is more distinct for ethanol compared to water, which is indicated by the much higher Weber number of ethanol. This leads to a faster atomization, and due to the larger radial velocity component induced by the nozzle flow, the surface waves grow in the jet specifically at the radial boundaries. This effect was less clear in previous investigations,[23,28] in which the surface tension difference between the liquids was not that distinct. Obviously, the aerodynamic breakup is more relevant in the near nozzle region in the present study due to the larger differences in surface tensions, which even complicates the jet breakup. The larger injection pressure leads to an increased velocity difference between spray and air so that these aerodynamic effects become more important. Consequently, the spray is pushed aside of its original propagation direction resulting in a broadened spray plume, which again supports aerodynamic breakup.

Additionally, the higher vapor pressure of ethanol leads to a higher probability of cavitation in the nozzle. Together with the lower Reynolds number and a transitional flow behavior, larger fluctuations in the spray shape can be observed and the angle increases. In general, the same trend was reported for the near-nozzle cone angle of DISI spray for a pressure change from 5 to 10 MPa.[56] There, an increased spray angle was observed for increased pressures as well. For water, a similar tendency is observed for the lower injection pressures, however, at 30 MPa injection pressure, the measurements reveal a lower

TABLE III. Average cone angles and 95% confidence intervals at 20 MPa.

	20 μs	120 μs	220 μs	320 μs
Ethanol	23.07° ± 0.56	33.08° ± 0.99	29.48° ± 0.59	29.85° ± 0.66
Water	22.13° ± 0.79	31.36° ± 0.85	28.98° ± 0.65	28.60° ± 0.62

angle for water than it was evaluated for 20 MPa. Payri *et al.* reported larger spray angles for larger injection pressures (30 and 60 MPa were studied for one liquid), which was explained by increasing cavitation tendency with pressure.[55]

In general, the increased confidence intervals for both liquids at higher pressures indicate a rise of the cyclic variations, which can be explained by larger wrinkling of the liquid surface in the near-nozzle region due to the aerodynamic breakup. The cyclic variations (in terms of 95% confidence interval) at 30 MPa are for ethanol 51.7% and for water 35.8% higher than at 20 MPa. These elevations in the cyclic variation cannot be explained by the nozzle flow since a larger Reynolds number due to larger flow velocity would imply a more stable flow behavior.

Regarding Feret's diameter of the liquid structures in the near-nozzle region up to 4 mm distance from the nozzle exit, no clear trend relating to the liquid properties could be observed for varied pressures at 220 μs. The time-dependent (left) and pressure (right) variation of the mean values including the 95% confidence intervals are presented in Fig. 10. The analyzed liquid structures show average dimensions of about 80–130 μm.

For water, the length of the liquid structures is reduced with an increase in the injection pressure. At high injection pressures, the flow is accelerated and the Reynolds number rises. The intensified turbulence and aerodynamic breakup results in smaller spray structures. Ethanol shows a different breakup behavior with larger structures at 20 MPa. At 30 MPa the turbulent and aerodynamic breakup predominates, which may be supported by cavitation-induced breakup, leading to smaller Feret's diameters.

At the incipient time step, high values for Feret's diameter with large fluctuations are observed. The images show only very little breakup of the jet and the (few) larger liquid structures explain the augmented confidence intervals. Due to further jet breakup because of the increased velocity when the needle is fully opened, the subsequent decline in the diameter was presumed. For the following time steps, the spray front exceeds the analyzed region, leading to a shift to slightly larger structures. In principle, the size of the liquid bodies is very similar for both liquids in the near-nozzle region. In Ref. 56, the differences in structural dimensions depending on the liquid viscosity and surface tension were also small, in general, although a higher number of large structures were observed for a higher viscous fuel with larger surface tension. Most probably, a larger number of images and measurement positions are necessary for clearer dependencies of Feret's diameter on the liquid properties. This analysis is conducted in the subsequent paragraphs.

To get better statistics for the structure sizes, the nozzle far-field was added to the analysis in another routine. With this method, up to around 2000 structures are evaluated in some of the investigated regions. In Fig. 11, the Feret's diameters for both, ethanol and water, downstream the nozzle exit are shown for all three investigated injection pressures at 220 μs. Due to the high surface tension of water and the resulting lower Weber number, a slower jet breakup is expected for water. Thus, compared to ethanol, larger liquid structures can be observed in the region from 5 up to 10 mm distance to the nozzle in all operating points. At 20 MPa, the difference is most distinct: The structures of water are about 116% larger on average compared to ethanol. Measurements of Kooji *et al.* showed the same tendency of smaller droplets with lower surface tension and thus a higher Weber number.[57] However, no primary spray structures were reported. At 30 MPa, larger structures can be found in the spray front, specifically for ethanol. This may be explained by the needle opening, which is much more forceful at higher pressures and may lead to a "blob"-injection. Please note that the position of the spray front is different for the various injection pressures (as the breakup distance of the spray is shorter at increased pressure).

Generally, the analyzed ligaments and clusters range from 20 μm up to 90 μm. The largest structures are perceived close to the nozzle, where liquid jet breakup scarcely starts. In a region 1 to 3 mm, only very few small droplets are separated from the spray core and can be recognized. After the breakup of the main jet at 3 to 5 mm distance from the nozzle exit, the average Feret's diameter decreases almost continually. In the spray front, most operating points show an increase in the structure size. These large structures are attributable to the behavior during the needle opening, which is still recognizable in the detected spray front region at 220 μs. However, also droplet coalescence and coagulation lead to an increase in the Feret's diameter at the denser spray front.

At all three injection pressures, water has a maximum in the Feret's diameter close to the nozzle. For ethanol, the peak is not as clearly apparent due to the different breakup behavior especially at 20 and 30 MPa. In Fig. 7, the contrast in atomization for both liquids is also visible in the single shot images and fits the analyzed data. Water tends to a complete disintegration into long, wavy ligaments and sheet-like structures, whereas ethanol breaks up into smaller clusters and droplets in the dense spray region. Additionally, due to the low

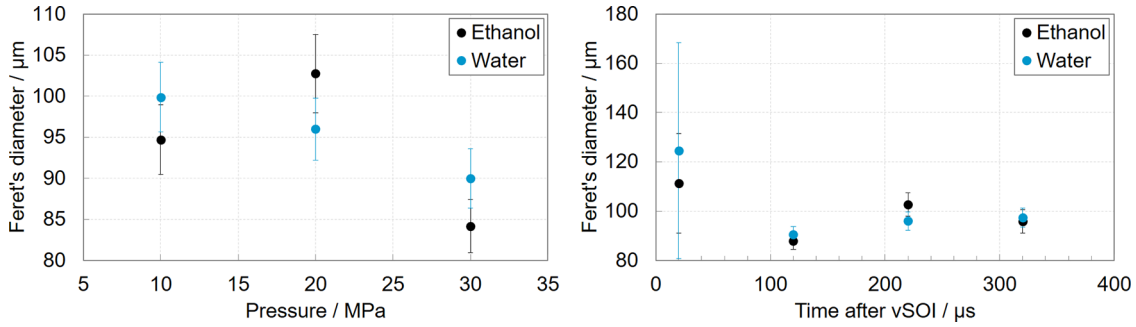

FIG. 10. Injection pressure dependent Feret's diameter at 220 μs (left) and time dependent Feret's diameter at 20 MPa (right) with 95% confidence interval. The measurement positions are up to 4 mm distance from the nozzle exit.

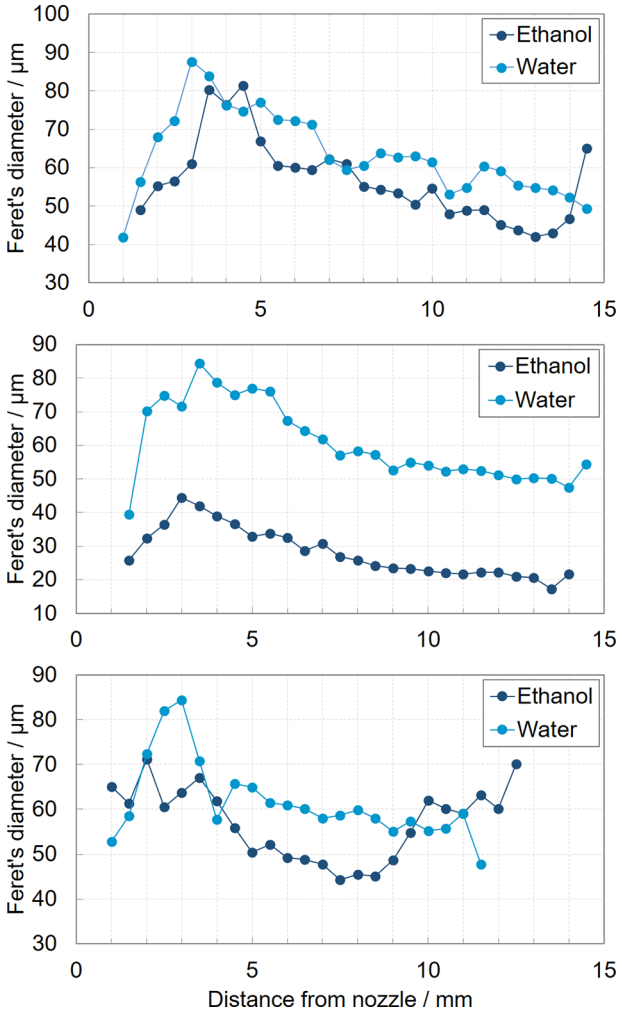

FIG. 11. Comparison of ligament sizes downstream the nozzle for water and ethanol at 10 MPa (top), 20 MPa (middle), and 30 MPa (bottom) and 220 μs after vSOI.

boiling temperature, droplets in the ethanol spray should evaporate faster than in a water spray. However, the evaporation enthalpy is also relatively large and for the large structures studied here, the evaporation should be insignificant. For example, the diameter of a 10 μm ethanol droplet is reduced due to evaporation by about 3.4% after 2 ms following Koegl *et al.*[58] under similar conditions, and the timescale studied here is maximal 320 μs.

Figure 12 shows these values of the Feret's diameter over nozzle distance at 10, 20, and 30 MPa for water on the left and ethanol on the right side. For water, the ligament sizes between 10 and 20 MPa differ mostly in the nozzle far field, whilst the difference is only of about 10 μm. The diameters are slightly smaller at a higher injection pressure, as assumed due to higher velocities and turbulences in the nozzle and therefore an increased Reynolds and Weber number. At 30 MPa the analysis reveals a faster atomization with a decrease in the ligament sizes close to the nozzle. Small diameters of around 60 μm are detected in the area from 4 mm to around 10 mm.

For ethanol shortly after the nozzle, a decline in diameter can be observed until large structures are detected in the spray front. For ethanol the ligament sizes at 20 MPa injection pressure differ most from the other measurements, revealing much lower values than all other considered operating points. On average ethanol showed about 24% smaller structures compared to the water spray for all investigated positions downstream the nozzle and injection pressures. This behavior could be explained due to different interfering effects. In comparison to water, the ethanol spray remains broader. However, the ethanol spray breaks up faster and into smaller structures, as indicated by the Ohnesorge number in Table I. In principle, this trend can be explained by the classical aerodynamic atomization theory, but additionally, the larger near-nozzle jet cone angle of ethanol supports the jet disintegration. Consequently, the differences of the Feret's diameter are smaller over the distance from the nozzle for ethanol, which is much more pronounced for water. At 20 MPa, in particular, the increased liquid momentum leads to more detected and smaller droplets, but the spay is not affected by the needle opening as much as at 30 MPa.

In general, we could observe relatively large structures also in downstream distances of 14 mm from the nozzle. Typically, they are not spherical, and consequently, they cannot be detected by conventional sizing techniques such as phase Doppler interferometry (PDI).

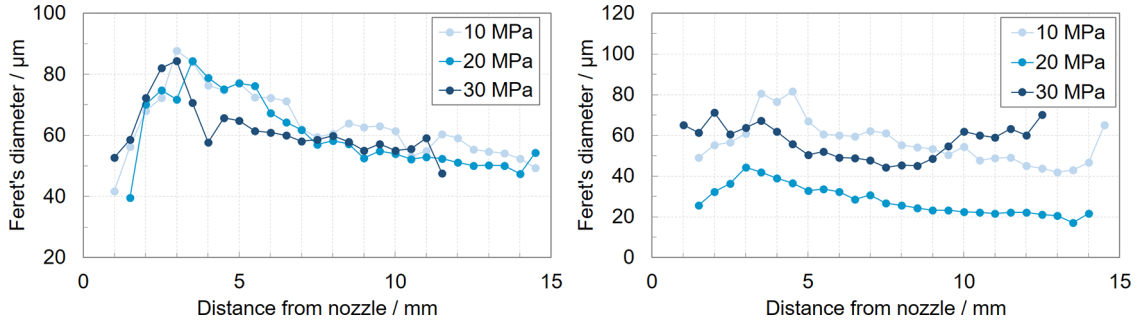

FIG. 12. Depiction of the ligament sizes in radial distance from the nozzle exit for water (left) and ethanol (right). For both liquids, three different injection pressures are considered at 220 μs after vSOI.

The largest structures were found at about 3 mm. After 7 mm (30 MPa) to 10 mm (10 MPa), no significant change of the size of large-scale structures occurs anymore. Droplets of smaller size ($< 20\,\mu$m) were not analyzed in the framework of this study as the focus was on primary spray structures. In general, there is almost no information on such spray structures available in the literature since most of these studies focus on droplet sizing using point-wise measurements based on PDI (or PDPA).[53,59]

CONCLUSIONS

The 2p-LIF approach was applied to a common DISI injector to quantitatively analyze the spray shape and primary spray structures depending on the liquid properties. A high-resolution imaging of the dense spray core enabled a comprehensive analysis of the atomization process close to the nozzle exit at different injection pressures. The recorded images were evaluated in terms of the cone angle and liquid structure lengths such as ligaments and clusters in the nozzle near-field. So far, there were almost no quantitative studies of primary spray structures to the best of the authors' knowledge. The basic model presumption from 2013[23] which predicts that higher viscosities will result in increased plume angles, could be verified and extended to much higher injection pressures (up to 30 MPa, i.e., ∼factor 3 larger) and Weber numbers (up to about 217 000, i.e., ∼factor 5 larger). It could also be proved that the surface tension and vapor pressure affect the cone angle less significantly. This model is in contrast to classical atomization models that just include aerodynamic breakup. Largest cyclic variations of the spray angle were observed during needle opening, i.e., early points in time after start of injection. Higher injection pressures showed larger cone angles and smaller liquid structures of the primary jet for both tested liquids. The atomization shows a main jet breakup distance of 7–10 mm, in which the structure sizes decreased drastically, especially for water. The jet breakup was much faster for ethanol, which showed on average about 24% smaller structures compared to the water spray for the studied injection pressures in the complete spray region. More homogeneous structural sizes and no clear main breakup distance could be observed for ethanol further downstream the nozzle. The injection pressure showed a relatively small effect on the dimensions of the primary structures for water. This effect was larger for ethanol, especially the larger injection pressure of 20 MPa resulted in about 50% smaller structures on average compared to 10 MPa.

In future work, it is necessary to study the effects of the nozzle flow in more detail, which requires optical accessible nozzles. Additionally, a combination of different optical diagnostics is required for better optical access of the spray, which could also allow tomography of several jets (such as x-ray tomography). The model should be tested for modern synthetic or biogenic fuels that can be better designed and varied regarding fuel properties. This could allow a better decoupling of different effects of the determining fuel properties, viscosity, vapor pressure, and surface tension for much deeper insights into nozzle flow and breakup processes.

ACKNOWLEDGMENTS

The authors gratefully acknowledge the financial support for parts of this work by the European Union's Horizon 2020 Research and Innovation programme under Grant Agreement No. 730871 (ARIES); the European Research Council (ERC) Starting Grant: "Spray-Imaging"—No. 638546; the Swedish Research Council (Nos. 2016–03894 and 2019–04784); and the Erlangen Graduate School in Advanced Optical Technologies (SAOT), which is funded by the state of Bavaria. We thank Ms. Sophie Sigl (FAU) for supporting the image post-processing and data analysis. Open Access funding provided by project DEAL. We acknowledge financial support by Universität der Bundeswehr München.

AUTHOR DECLARATIONS

Conflict of Interest

The authors have no conflicts to disclose.

Author Contributions

Hannah Ulrich: Data curation (equal); Formal analysis (lead); Investigation (equal); Software (lead); Validation (lead); Visualization (lead); Writing – original draft (lead); Writing – review and editing (lead). **Bastian Lehnert:** Data curation (equal); Investigation (equal); Software (supporting); Validation (supporting). **Diego Guénot:** Investigation (equal). **Kristoffer Svendsen:** Investigation (equal). **Olle Lundh:** Conceptualization (equal); Resources (equal); Supervision (equal). **Michael Wensing:** Resources (equal); Supervision (equal). **Edouard Berrocal:** Conceptualization (equal); Funding acquisition (lead); Investigation (supporting); Methodology (equal); Project administration (equal); Resources (equal); Supervision (equal); Visualization (equal); Writing – original draft (supporting). **Lars Zigan:** Conceptualization (equal); Funding acquisition (equal); Methodology (equal); Project administration (lead); Supervision (equal); Writing – original draft (supporting); Writing – review and editing (supporting).

DATA AVAILABILITY

The data that support the findings of this study are available from the corresponding author upon reasonable request.

REFERENCES

[1]N. Ashgriz, *Handbook of Atomization and Sprays: Theory and Applications* (Springer, New York, 2011).
[2]G. O. Erol, J. Hasslberger, M. Klein, and N. Chakraborty, "A direct numerical simulation analysis of spherically expanding turbulent flames in fuel droplet-mists for an overall equivalence ratio of unity," Phys. Fluids **30**, 086104 (2018).
[3]L. Angelilli, P. P. Ciottoli, F. Picano, M. Valorani, and H. G. Im, "Assessment of subgrid dispersion models for large eddy simulations of turbulent jet flows with dilute spray droplets," Phys. Fluids **34**, 073305 (2022).
[4]F. Ferraro, S. Gierth, S. Salenbauch, W. Han, and C. Hasse, "Soot particle size distribution reconstruction in a turbulent sooting flame with the split-based extended quadrature method of moments," Phys. Fluids **34**, 075121 (2022).
[5]M. Koegl, B. Hofbeck, S. Will, and L. Zigan, "Investigation of soot formation and oxidation of ethanol and butanol fuel blends in a DISI engine at different exhaust gas recirculation rates," Appl. Energy **209**, 426 (2018).
[6]Y. Liu and B. Derby, "Experimental study of the parameters for stable drop-on-demand inkjet performance," Phys. Fluids **31**, 032004 (2019).
[7]A. Sankaran, J. Wu, R. Granda, V. Yurkiv, F. Mashayek, and A. L. Yarin, "Drop impact onto polarized dielectric surface for controlled coating," Phys. Fluids **33**, 062101 (2021).
[8]K. Meng, L. Li, X. Zhang, Z. Huang, F. Wang, R. Li, and Q. Lin, "Comparison of combustion and micro-explosion characteristics of droplet group of biodiesel/ethanol and biodiesel/RP-3/ethanol," Phys. Fluids **34**, 061903 (2022).
[9]I. Qavi and L. Jiang, "Optical characterization of near-field sprays for various alternative and conventional jet fuels using a flow-blurring injector," Flow, Turbul. Combust. **108**, 599 (2022).

[10]V. Dorfner, J. Domnick, F. Durst, and R. Kohler, "Viscosity and surface tension effects in pressure swirl atomization," Atomization Sprays **5**, 261 (1995).
[11]T. G. Theofanous and G. J. Li, "On the physics of aerobreakup," Phys. Fluids **20**, 052103 (2008).
[12]W. Zhu, N. Zhao, X. Jia, X. Chen, and H. Zheng, "Effect of airflow pressure on the droplet breakup in the shear breakup regime," Phys. Fluids **33**, 053309 (2021).
[13]R. D. Reitz, "Modeling atomization processes in high-pressure vaporizing sprays," Atomisation Spray Technol. **3**, 309 (1987).
[14]O. Desjardins, G. Blanquart, G. Balarac, and H. Pitsch, "High order conservative finite difference scheme for variable density low Mach number turbulent flows," J. Comput. Phys. **227**, 7125 (2008).
[15]A. Fath, "Charakterisierung Des Strahlaufbruch-Prozesses Bei Der Instationären Druckzerstäubung," Dissertation (FAU Erlangen-Nürnberg/ESYTEC-Verlag, Erlangen, 1997).
[16]X. Jiang, G. A. Siamas, K. Jagus, and T. G. Karayiannis, "Physical modelling and advanced simulations of gas–liquid two-phase jet flows in atomization and sprays," Prog. Energy Combust. Sci. **36**, 131 (2010).
[17]K. Y. Huh and A. D. Gosman, in "Phenomenological model of diesel spray atomisation," in Proceedings of the international Conference on Multiphase Flows, Tsukuba, Japan, 24–27 September 1991, pp. 515–518.
[18]G. Stiesch, *Modeling Engine Spray and Combustion Processes* (Springer, Berlin, 2003).
[19]A. Sou, S. Hosokawa, and A. Tomiyama, "Effects of cavitation in a nozzle on liquid jet atomization," Int. J. Heat Mass Transfer **50**, 3575 (2007).
[20]R. D. Reitz, "Mechanism of atomization of a liquid jet," Phys. Fluids **25**, 1730 (1982).
[21]M. Hosbach, R. Skoda, T. Sander, U. Leuteritz, and M. Pfitzner, "On the temperature influence on cavitation erosion in micro-channels," Exp. Therm. Fluid Sci. **117**, 110140 (2020).
[22]D. Guénot, K. Svendsen, B. Lehnert, H. Ulrich, A. Persson, A. Permogorov, L. Zigan, M. Wensing, O. Lundh, and E. Berrocal, "Distribution of liquid mass in transient sprays measured using laser-plasma-driven x-ray tomography," Phys. Rev. Appl. **17**, 064056 (2022).
[23]L. Zigan, J.-M. Shi, I. Krotow, I. Schmitz, M. Wensing, and A. Leipertz, "Fuel property and fuel temperature effects on internal nozzle flow, atomization and cyclic spray fluctuations of a direct injection spark ignition–injector," Int. J. Engine Res. **14**, 543 (2013).
[24]A. Andriotis, M. Gavaises, and C. Arcoumanis, "Vortex flow and cavitation in diesel injector nozzles," J. Fluid Mech. **610**, 195 (2008).
[25]D. Mamaikin, T. Knorsch, P. Rogler, J. Wang, and M. Wensing, "The effect of transient needle lift on the internal flow and near-nozzle spray characteristics for modern GDI systems investigated by high-speed X-ray imaging," Int. J. Engine Res. **23**, 300 (2022).
[26]M. M. Tareq, R. A. Dafsari, S. Jung, and J. Lee, "Effect of the physical properties of liquid and ALR on the spray characteristics of a pre-filming airblast nozzle," Int. J. Multiphase Flow **126**, 103240 (2020).
[27]L. Lešnik, B. Kegl, G. Bombek, M. Hočevar, and I. Biluš, "The influence of in-nozzle cavitation on flow characteristics and spray break-up," Fuel **222**, 550 (2018).
[28]R. Torelli, S. Som, Y. Pei, Y. Zhang, and M. Traver, "Influence of fuel properties on internal nozzle flow development in a multi-hole diesel injector," Fuel **204**, 171 (2017).
[29]T. D. Fansler and S. E. Parrish, "Spray measurement technology: A review," Meas. Sci. Technol. **26**, 012002 (2015).
[30]E. Berrocal, C. Conrad, J. Püls, C. L. Arnold, M. Wensing, M. Linne, and M. Miranda, "Two-photon fluorescence laser sheet imaging for high contrast visualization of atomizing sprays," OSA Continuum **2**, 983 (2019).
[31]D. Guénot, K. Svendsen, J. Björklund Svensson, H. Ekerfelt, A. Persson, O. Lundh, and E. Berrocal, "Simultaneous laser-driven x-ray and two-photon fluorescence imaging of atomizing sprays," Optica **7**, 131 (2020).
[32]A. Coghe and G. E. Cossali, "Quantitative optical techniques for dense sprays investigation: A survey," Opt. Lasers Eng. **50**, 46 (2012).
[33]M. Linne, "Imaging in the optically dense regions of a spray: A review of developing techniques," Prog. Energy Combust. Sci. **39**, 403 (2013).
[34]M. Rahm, M. Paciaroni, Z. Wang, D. Sedarsky, and M. Linne, "Evaluation of optical arrangements for ballistic imaging in sprays," Opt. Express **23**, 22444 (2015).
[35]E. Berrocal, E. Kristensson, P. Hottenbach, M. Aldén, and G. Grünefeld, "Quantitative imaging of a non-combusting diesel spray using structured laser illumination planar imaging," Appl. Phys. B **109**, 683 (2012).
[36]T. Breuninger, K. Greger, and E. H. K. Stelzer, "Lateral modulation boosts image quality in single plane illumination fluorescence microscopy," Opt. Lett. **32**, 1938 (2007).
[37]E. Berrocal, E. Kristensson, and L. Zigan, "Light sheet fluorescence microscopic imaging for high-resolution visualization of spray dynamics," Int. J. Spray Combust. Dyn. **10**, 86 (2018).
[38]C. Xu, W. Zipfel, J. B. Shear, R. M. Williams, and W. W. Webb, "Multiphoton fluorescence excitation: new spectral windows for biological nonlinear microscopy" Proc. Natl. Acad. Sci. U. S. A. **93**, 10763 (1996).
[39]J. H. Frank, X. Chen, B. D. Patterson, and T. B. Settersten, "Comparison of nanosecond and picosecond excitation for two-photon laser-induced fluorescence imaging of atomic oxygen in flames," Appl. Opt. **43**, 2588 (2004).
[40]W. D. Kulatilaka, B. D. Patterson, J. H. Frank, and T. B. Settersten, "Comparison of nanosecond and picosecond excitation for interference-free two-photon laser-induced fluorescence detection of atomic hydrogen in flames," Appl. Opt. **47**, 4672 (2008).
[41]D. R. Richardson, S. Roy, and J. R. Gord, "Femtosecond, two-photon, planar laser-induced fluorescence of carbon monoxide in flames," Opt. Lett. **42**, 875 (2017).
[42]C. K. Law, C. H. Lee, and N. Srinivasan, "Combustion characteristics of water-in-oil emulsion droplets," Combust. Flame **37**, 125 (1980).
[43]B. Franzke, T. Voßhall, P. Adomeit, and A. Müller, "Water injection for meeting future RDE requirements for turbocharged gasoline engines," MTZ Worldwide **80**, 30 (2019).
[44]M. Koegl, C. Mull, Y. N. Mishra, S. Will, and L. Zigan, "Characterization of fuel/water mixtures and emulsions with ethanol using laser-induced fluorescence," Appl. Opt. **59**, 1136 (2020).
[45]K. Svendsen, I. G. González, M. Hansson, J. B. Svensson, H. Ekerfelt, A. Persson, and O. Lundh, "Optimization of soft X-ray phase-contrast tomography using a laser wakefield accelerator," Opt. Express **26**, 33930 (2018).
[46]M. Zantow, R. Dendere, and T. S. Douglas, in *Annual International Conference of the IEEE Engineering in Medicine and Biology Society* (IEEE, 2013), p. 1776.
[47]A. Asgarian, Z. Yang, Z. Tang, M. Bussmann, and K. Chattopadhyay, "An image feature consolidation technique (IFCT) to capture multi-range droplet size distributions in atomizing liquid sheets," Exp. Fluids **61**, 1–22 (2020).
[48]L. P. Chin, P. G. LaRose, R. S. Tankin, T. Jackson, J. Stutrud, and G. Switzer, "Droplet distributions from the breakup of a cylindrical liquid jet," Phys. Fluids A **3**, 1897 (1991).
[49]J. A. Dean and N. A. Lange, *Lange's Handbook of Chemistry* (McGraw-Hill, New York, 1999).
[50]E. W. Lemmon, M. L. Huber, and M. O. McLinden, "REFPROP 9.1, Reference Fluid Thermodynamic and Transport Properties Database" (NIST, 2013).
[51]S. Bornschlegel, C. Conrad, A. Durst, J. Wang, and M. Wensing, "Multi-hole gasoline direct injection: In-nozzle flow and primary breakup investigated in transparent nozzlesand with X-ray," Int. J. Engine Res. **19**, 67 (2018).
[52]A. Neubauer, "Messtechnische Erfassung primärer Strahlstrukturen von Benzin- und Dieselsprays," Dissertation (FAU Erlangen-Nürnberg, Erlangen, 2020).
[53]J. Shin, D. Kim, J. Seo, and S. Park, "Effects of the physical properties of fuel on spray characteristics from a gas turbine nozzle," Energy **205**, 118090 (2020).
[54]L. Zigan, I. Schmitz, A. Flügel, M. Wensing, and A. Leipertz, "Structure of evaporating single- and multicomponent fuel sprays for 2nd generation gasoline direct injection," Fuel **90**, 348 (2011).
[55]F. Payri, V. Bermúdez, R. Payri, and F. J. Salvador, "The influence of cavitation on the internal flow and the spray characteristics in diesel injection nozzles," Fuel **83**, 419 (2004).
[56]L. Zigan, I. Schmitz, M. Wensing, and A. Leipertz, in 23rd Annual Conference on Liquid Atomization and Spray Systems, 2010.
[57]S. Kooij, R. Sijs, M. M. Denn, E. Villermaux, and D. Bonn, "What determines the drop size in sprays?," Phys. Rev. X **8**, 031019 (2018).
[58]M. Koegl, Y. N. Mishra, K. Baderschneider, C. Conrad, B. Lehnert, S. Will, and L. Zigan, "Planar droplet sizing for studying the influence of ethanol admixture on the spray structure of gasoline sprays," Exp. Fluids **61**, 209 (2020).
[59]Z. Zhang and S. Ziada, "PDA measurements of droplet size and mass flux in the three-dimensional atomisation region of water jet in air cross-flow," Exp. Fluids **28**, 29 (2000).